Eur. Phys. J. D **21**, 353–359 (2002)
DOI: 10.1140/epjd/e2002-00193-0

THE EUROPEAN PHYSICAL JOURNAL D

High order harmonic generation optimization with an apertured laser beam

S. Kazamias[a], F. Weihe, D. Douillet, C. Valentin, T. Planchon, S. Sebban, G. Grillon, F. Augé, D. Hulin, and Ph. Balcou

Laboratoire d'Optique Appliquée, ENSTA-École Polytechnique[b], 91761 Palaiseau Cedex, France

Received 31 May 2002
Published online 24 September 2002 –

Abstract. We report a systematic study of high order harmonic generation with an infrared laser apertured by an iris, as a function of the aperture size. Measurements were made of harmonic generation efficiency for different gas species, laser energies and focal geometries. Harmonic efficiencies as a function of aperture show a characteristic peaked shape, which is independent of gas species and harmonic order. A one dimensional, time dependent simulation of harmonic generation in a gas cell, taking into account experimentally measured transverse coherence of the laser, closely reproduces the observed behaviours. We show that the aperture diameter which maximizes harmonic yield is the result of a compromise between considerations of focal geometry and ionization (which favour small apertures); and harmonic dipole amplitude and phase (which favour large apertures).

PACS. 32.80.Rm Multiphoton ionization and excitation to highly excited states (e.g., Rydberg states) – 42.65.Ky Harmonic generation, frequency conversion

1 Introduction

The generation of high-order harmonics (HHG) of intense, short pulse laser radiation is both itself a subject of scientific study, and a unique, short-wavelength light source with many potential applications. To generate high harmonics, lasers can interact with gas targets in a number of different geometries, each with consequences for the HHG process. In many HHG experiments, the laser interacts with the nonlinear medium within a hollow waveguide, which controls many aspects of the interaction and propagation geometry [1,2]. For other studies and applications, the unguided laser beam is focused into a gas jet, or a gas-filled cell. In these cases the focal geometry of the laser will dominate many aspects of HHG, affecting propagation, and thus influencing conversion efficiencies. To optimize the yield of high-order harmonic generation in a non-waveguide gas target, an iris is often used to aperture the infrared beam before it is focused into the gaseous medium [3,4]. The role of the aperture in improving HHG fluxes is often not explained, or if it is discussed, the explanation is usually given informally in terms of either the increase of the interaction volume or the reduction of the geometrical phase-mismatch. These arguments have only qualitative validity; a more sophisticated treatment, including these and other effects, is required to explain the behavior of HHG as a function of beam aperture.

We present here the first systematic study of the complex influence of truncating the beam on parameters important to HHG, including the single-atom HHG process, volume effects, and phase matching. At a time when applications of harmonic radiation are developing at a rapid pace, understanding the roles of the experimental parameters which critically affect HHG conversion efficiency is of increasing importance in the growing field of ultrafast, short-wavelength optics. We experimentally observed an improvement in harmonic flux, by a factor up to 10, when the aperture diameter is reduced. A peak in efficiency is observed for an aperture diameter of approximately half of the laser beam diameter. With our laser parameters, this result is quite robust, depending strongly on neither the gas species nor the harmonic order. By reducing the transmitted energy and also changing the focal geometry, focused intensity is reduced. This affects ionization rates [5,6], and therefore the refractive index of the gas; and the amplitude and phase of the induced harmonic dipole [7,8]. Increasing the focal volume may increase the volume in which a particular harmonic order is generated. Changing the focal geometry also alters the Gouy phase shift gradient [9]. Finally, the diffraction of the laser by the circular aperture can not be neglected, and the modifications of the Strehl ratio when only the central part of the beam is selected should be considered. We modeled our experimental observations with a time-dependent simulation of the harmonic generation process, taking into account the above considerations, including propagation

[a] e-mail: kazamias@ensta.fr
[b] UMR 7639 du CNRS

and phase-matching effects; the results are in excellent agreement with our measurements.

The outline of the paper is the following. In Section 2 we describe the experimental arrangement for generating harmonics and an overview of experimental observations, including HHG efficiency and the behavior of HHG with a truncated beam. Section 3 contains a discussion of the geometry of laser beam propagation and focusing, including the consideration of the laser wavefront. In Section 4 we describe the numerical simulation. We discuss the role of different parameters on phase matching in order to explain the presented results.

2 Experimental set-up and typical behaviour

2.1 Set-up

We have performed a systematic study of aperturing on high harmonics generated with a Ti:sapphire laser system delivering a 1 kHz train of 6 mJ, 30 fs pulses with a center wavelength of 810 nm. The beam has an initial diameter of 22 mm ($1/e^2$), which is the iris diameter for which the energy transmission is 86% [10]. After passing through a variable-diameter aperture, the truncated beam is focused by a 1 m focal length MgF_2 lens into a vacuum system containing a quasi-static gas cell near the vacuum focal position of the laser. The gas species, gas pressure, cell length, and the position of the focus relative to the cell, are all easily variable parameters. The harmonics generated in the gas cell co-propagate with the laser until the infrared radiation is blocked after 1 m by two 150 nm thick aluminum filters, which pass approximately 30% of the vacuum ultraviolet (VUV) radiation in a spectral band from *ca.* 20 eV to 70 eV. The harmonic spectrum is then analyzed by a transmission-grating VUV/XUV spectrometer coupled to an XUV–CCD camera detector. Careful calibrations of each element in the spectrometer allow us to infer absolute photon numbers from the spectra. Harmonic spectra recorded represent averages over many laser shots (100 to 5 000 shots, depending on harmonic radiation signal levels).

2.2 HHG flux and conversion efficiency

Figure 1 presents in gray line the harmonic spectrum obtained in argon with the fully open laser beam, and in black line the spectrum obtained with a beam apertured down to 10 mm. An increase by a factor of 10 is clear on harmonics 23 to 27; however, the extent of the plateau is larger on the fully-open diaphragm spectrum, corresponding to higher intensities at focus. Harmonic radiation is then generated the most efficiently at higher orders (20–25 nm) as expected. Moreover, the shape of the spectrum of each harmonic is qualitatively different: blue shifting of the harmonic lines is obvious on the wide diaphragm spectrum, as well as a complicated spectral structures related to multiple quantum paths [8].

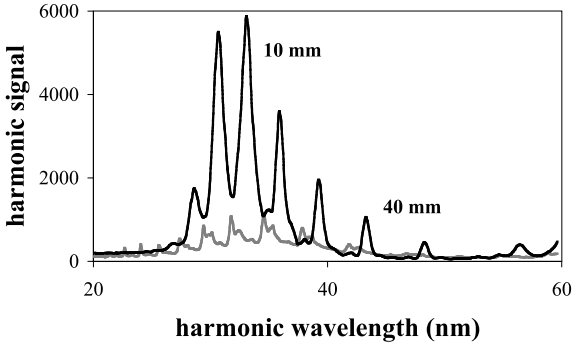

Fig. 1. Typical spectra obtained in argon for a wide open iris (40 mm, grey line) and for a closer one (10 mm, dark line).

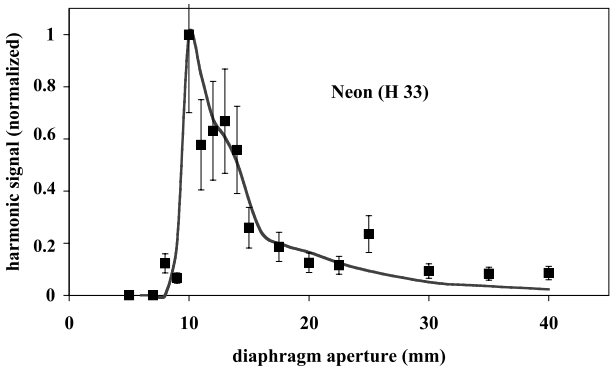

Fig. 2. Black squares: experimental harmonic signal for the 33rd harmonic order in neon as a function of diaphragm aperture. Thick line: theoretical simulations with the same generation conditions (10 torr, 2 mm long cell, focus at the entrance, 6 mJ total laser energy).

We have performed a systematic optimization of conversion efficiency, defined as the ratio of the energy in the harmonic pulse with respect to that of the transmitted laser beam at focus, with respect to the diaphragm diameter. The maximum number of photons of harmonic radiation obtained per shot in argon was about 10^{10} photons per harmonic in the range of 30–40 nm, representing conversion efficiencies up to 2×10^{-5}; conversion efficiencies for xenon are comparable for a range of lower harmonic orders (40–50 nm). For neon, the conversion efficiency is lower, as can be expected: 7×10^{-8} was obtained for the most efficient harmonic.

2.3 Behaviour of HHG with a truncated beam

We present in Figures 2 to 4 the dependence of the harmonic signal of harmonics 33, 21 and 19 generated in Ne, Ar and Xe respectively (experimental points in black squares), *versus* the iris size. The data are obtained in a 2 mm long gas cell filled with 10 torr of gas, with the vacuum laser focus located at the entrance of the cell.

The maximum intensity at focus of the un-apertured laser beam is estimated to 2×10^{15} W/cm^2, taking into account the experimental Strehl ratio, *i.e.* the ratio between the maximum intensity reached by the aberrated

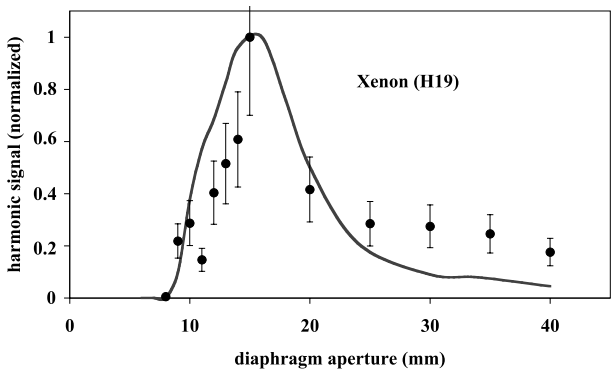

Fig. 3. Black circles: experimental harmonic signal for the 19th harmonic order in xenon as a function of diaphragm aperture. Thick line: theoretical simulations with the same generation conditions (10 torr, 2 mm long cell, focus at the entrance, 6 mJ total laser energy).

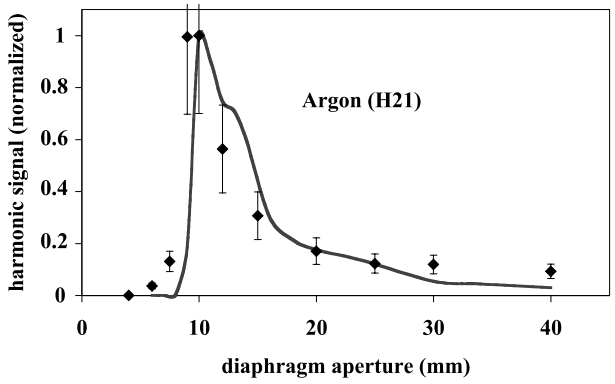

Fig. 4. Black squares: experimental harmonic signal for the 21st harmonic in argon as a function of diaphragm aperture. Thick line: theoretical simulations with the same generation conditions (10 torr, 2 mm long cell, focus at the entrance, 6 mJ total laser energy).

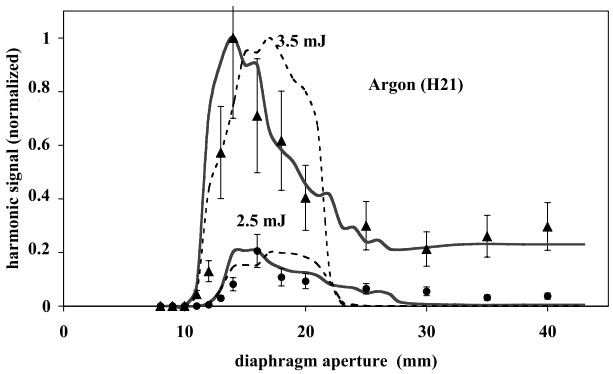

Fig. 5. Comparisons of the harmonic signal as a function of aperture size, for different laser incident energies. Triangles and circles: experimental harmonic signals for the 21st harmonic in argon as a function of diaphragm aperture, with respectively 3.5 mJ and 2.5 mJ total laser energy. Thick line: theoretical simulations with the same generation conditions (15 torr, 5 mm long cell, focus 8mm before the entrance).

laser beam, and those that would be obtained by a perfect diffraction-limited laser beam. This ratio is estimated to 40% from wavefront measurements. This high intensity value is occasionally used in harmonic generation studies [11].

The error bars on the harmonic signal are large, 30%, because of the shot-to-shot instabilities of the laser, which induce larger instabilities on the HHG levels due to the highly nonlinear nature of the HHG process. The curves display a characteristic behaviour, consisting of a sharp rise for narrow diaphragms, open to only half of the full aperture here, followed by a slower decrease up to full aperture. For clarity, data for only one order (the 33rd in Ne and 19th in Xe) are displayed; exactly the same behaviours are observed for all harmonic orders within the plateau. In fact, as we discuss below, even for different gases the behavior is qualitatively the same, and only varies quantitatively.

For small diaphragm apertures compared to the laser waist, the focused intensity scales as the fourth power of diaphragm diameter. Indeed, the energy transmission is approximately quadratic with respect to the iris diameter, whereas the focal spot size decreases quadratically. This rapid variation in terms of intensity when the iris is slightly opened explains why the maximum is reached so abruptly, in particular for light gases like neon. One very surprising feature however, is the position of the maximum in Figure 3 as compared to Figure 2: the optimum diaphragm in xenon is larger than in neon, so that the optimum in xenon corresponds to higher intensities than in neon. There is here an apparent contradiction with the well-known fact that making high harmonics in neon requires much larger intensities than in xenon.

Figure 5 shows how the characteristic behaviour is modified as the incident laser energy is reduced, while keeping all other geometrical conditions identical. As can be expected, the value of the optimal diaphragm is larger, and the best photon flux is strongly reduced. The conversion efficiency itself considerably decreases with the laser energy. In the generation conditions presented here, the maximum conversion efficiency as a function of the iris aperture is up to 10^{-5} at a laser energy of 6 mJ, it goes down to 4×10^{-6} at 4 mJ and to 10^{-6} at 2.5 mJ. Note that the maximum intensity at focus with 2 mJ and a fully open iris is already higher than typical intensities for HHG.

The energy dependent shape of the diaphragm curve displayed in Figure 5, leading to unexpected optimal diameter values, the severe drop in conversion efficiency when the incident energy is reduced, must all be related to complex macroscopic geometrical effects such as volume effects, or phase matching. To be able to model such effects, we have first investigated in details both experimentally and numerically the various geometrical changes to the laser beam caused by aperturing.

3 Geometrical effects of the iris aperture on the infrared beam

We can distinguish three major consequences of aperturing the beam: the variation of the transmitted laser energy and how it is distributed over the focal region; the variation of the focusing phase (Gouy phase) that plays a major role in phase matching; and the modification of the quality of the transmitted wavefront for a realistic experimental laser beam. These three aspects are considered in turn.

3.1 Energy transmission and focus geometry

We have first measured the parameters of the infrared laser beam. The waist w_0 of the unfocused laser beam is 11 mm. We checked that the transmission of the iris as a function of the aperture diameter $2a$ is well reproduced by the well-known formula for the transmission of a TEM00 Gaussian transverse mode through a circular aperture [10]:

$$T = 1 - \mathrm{e}^{-2a^2/w_0^2}. \quad (1)$$

Reducing the apertured beam diameter also increases the focal volume both transversely and longitudinally, this can be evaluated using a diffraction integral giving the field amplitude as a function of the distance to the focus [12]. We can infer an equivalent waist w of the focal spot, as the radius for which the intensity drops to $1/e^2$ of the central value, and an equivalent Rayleigh range z_R as the distance on axis for which the intensity is divided by 2.

3.2 Gouy phase variation

Focusing induces a geometrical phase slip, known as the Gouy phase, over a typical distance of the Rayleigh range z_R, that scales quadratically with the focal spot size w. However this variation of the laser phase along the propagation axis is not strictly equivalent in the case of a purely Gaussian beam, and in that of a truncated (almost top-hat) beam. For the sake of clarity, let us define the Gouy dephasing length as the inverse of the Gouy phase gradient at focus:

$$L_\mathrm{G} = 1/(\partial\phi/\partial z). \quad (2)$$

This Gouy dephasing length, characterizing the π phase slip at focus, is simply equal to the Rayleigh range characterizing the on-axis intensity variation for a Gaussian beam: $L_\mathrm{G} = z_\mathrm{R}$. Using diffraction integrals, we can simply evaluate L_G in the case of a truncated beam. The numerical ratio between L_G and z_R is found to deviate rapidly from 1, and stabilizes around 1.3. This parameter influences the one dimensional efficiency of harmonic generation *via* macroscopic, on axis phase matching effects: for a given transmitted energy, the Gouy dephasing length will be longer for a truncated beam than for a purely Gaussian beam giving the same focused intensity.

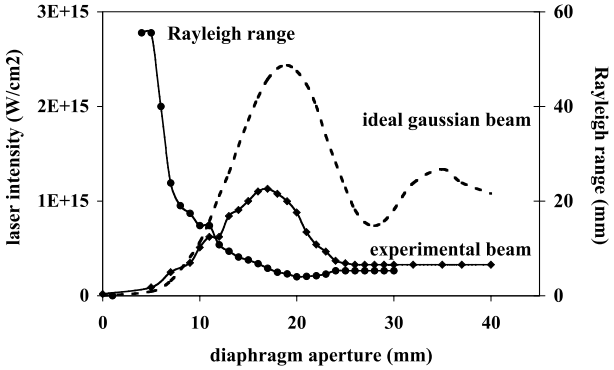

Fig. 6. Full squares: on axis maximum laser intensity at 8 mm from the focus inferred from Shack-Hartmann measurements of the experimental laser wavefront. Dashed line: theoretical results with a Gaussian beam. Full circles: Rayleigh range in mm.

3.3 Shack Hartmann determination of the phase-fronts

The previous calculations were based on the assumption of having a perfectly diffraction limited laser beam, which in most experimental cases is simply unrealistic. This could be an important problem for theory/experiment comparisons, as a precise evaluation of the on axis intensity and focus geometry is required to get reasonable prediction of HHG efficiency. Indeed, wavefront defects are known to induce significant discrepancies between predicted and experimental intensity profiles. It is therefore necessary to get a realistic estimation of the corresponding ratio, known as the Strehl ratio.

To this aim, we performed accurate measurements of the laser wavefront with a Shack-Hartmann wavefront sensor [13]. These far-field measurements were then used as initial conditions in a numerical beam propagation software package (Commod Pro [18]) to observe the consequences of wavefront imperfections on important beam parameters at focus.

The on axis intensity, displayed in Figure 6, differs strongly between the theoretical Gaussian case (solid line) and our experimental conditions (dashed line). In particular, for large diaphragms the perfect Gaussian case exhibits a ripple due to a Fresnel-like interference on axis, while in the experimental case the intensity is constant for diaphragm larger than the laser waist. The wavefront quality is indeed known to be poor far from axis, and better closer to it. As a result, apart from minor calibration problems, the Gaussian and experimental results are similar for narrow diaphragms. In contrast, the experimental Rayleigh range z_R and Gouy dephasing lengths thus calculated are essentially unchanged from the perfect Gaussian treatment.

Following this experimental approach, we have obtained tables of on axis intensities, Rayleigh ranges and Gouy dephasing lengths, allowing us in turn to derive ionization rates and harmonic dipoles which enter into the following calculation of HHG yields.

4 Harmonic generation and propagation

4.1 Description of the numerical model

In order to model the experimental data, we developed a one-dimensional model similar in spirit to the one proposed by Durfee *et al.* [14] in hollow core fibers, but modified to take into account (i) the freely propagating nature of the propagating beam, and (ii) the diaphragm-dependent transverse extent of the beam. In our model, the harmonic signal is computed as the time-integrated product of a non-linear polarization, a phase-matching and absorption factor, and a transverse cross-sectional factor describing the size of the polarization.

The non-linear polarization $d(t)$ stems from the Lewenstein model [7], from which the intensity and phase dependence of the polarization along one quantum path is derived. In the following, we consider by default the second quantum path. Taking as an example the case of argon at intensities below 2×10^{14} W/cm^2, we thus consider an atomic phase varying as $-25.4I$ (in units of 10^{14} W/cm^2, [20]), and a non linear dipole amplitude increasing as I^9 below the cutoff/plateau transition, and as I^3 above.

The variation of the transverse cross sectional area over which a given harmonic is efficiently generated is related to that of the laser waist with the iris aperture. This area scales as the inverse of the iris aperture for small diameters. We consider πw^2 as the relevant parameter for our model, where w is obtained from the method described in Section 3.

Finally, we perform a one-dimensional calculation of the time varying mismatch between the phase of the harmonic radiation of a given order, and that of the infrared laser. This mismatch δk is the result of the contributions of the Gouy phase induced by focusing the infrared beam but also the electronic dispersion due to ionization, and the atomic phase (intrinsic phase of the harmonic radiation) [8]. The result can be expressed in terms of propagation wave-vectors as follows [9]:

$$\delta k = \nabla\phi_q = k_q - qk_{\text{laser}} + \nabla\phi_{\text{at}}, \tag{3}$$

where q is the harmonic order, k_q the qth harmonic wavevector, k_{laser} the laser wavevector.

From the plasma dispersion formula, we have:

$$n_{\text{laser}} = 1 - \frac{n_e}{2n_c(\omega_{\text{laser}})}, \tag{4}$$

where n_e is the ionization probability and n_c the critical plasma density at a given wavelength. We neglect the plasma dispersion at the harmonic wavelength ($k_q = q\omega/c$). The influence of focusing the laser on k_{laser} is taken into account by the Gouy phase gradient (see Sect. 3.2). Equation (3) can then be simplified into:

$$\delta k = q\frac{\omega}{c}\frac{n_e}{2n_c} + q\nabla\phi_{\text{G}} + \nabla\phi_{\text{at}}. \tag{5}$$

Strictly speaking, each of these wavevectors is defined locally, and may thus vary along the axis in the medium. They are closely related to laser intensity and electron density which are strongly z-dependent. Two cases may happen here. If, at a given time t in the pulse, the total wavevector $\delta k(t)$ happens to present negligible variations along z, then the phase mismatch between laser polarization and harmonic field can be expressed as

$$\phi(q)(t) = \delta k(t)z = \pi z/L_{\text{coh}}(t). \tag{6}$$

Phase matching calculations can then be performed analytically. Consequently, the number of photons emitted on axis per unit of time and of area for a given harmonic order is given by [15] in a one dimensional model, taking absorption into account by the use of L_{abs} (distance over which the emitted radiation is absorbed by a factor $1/e$ by the generating gas).

This is achieved when the Rayleigh range is large compared to the cell length (z_{R} is the natural evolution distance for both atomic and Gouy phase), that is appropriate to small diaphragm apertures. The last expression of harmonic flux has been used for the fits of Figures 2, 4 and 3, for which the cell length was only 2 mm and the cell was placed at the focus where the atomic phase contribution is negligible. We have checked numerically that, in such conditions, the linear phase approximation is accurate enough, even for larger iris apertures.

Conversely, for long cell lengths and shorter Rayleigh ranges, the spatial variations of $\delta k(t)$ may prevent to use this approximation. In such a case, there is no other solution than resorting to the full integration along z of the phase mismatch $\phi_q(t)$:

$$\left|\int_0^{L_{\text{med}}} d(z)\exp\left(-\frac{L_{\text{med}}-z}{2L_{\text{abs}}}\right)\exp(\text{i}\phi_q(z)\text{d}z\right|^2. \tag{7}$$

This turned out to be necessary for the fits of Figure 5, displaying results taken with a long cell length (5 mm) and a cell location 8 mm after the focus. The full treatment of equation (7) was therefore used. In practice, the first step of the code is the solution of the system of differential equations, based on the ADK rates [5], evaluated with the time varying envelope of the pulse. It provides the instantaneous ionization level of the medium from which the coherence length is deduced. From the ionization level, the neutral density can be used to evaluate the absorption length; the one-dimensional propagation factor of equation (7) can therefore be deduced.

Figure 7 displays the time evolution of the coherence length, calculated for the 21st harmonic of argon, considering a 10 mm diameter iris and a gas pressure of 10 torr. It can be compared to the laser intensity envelope (thin line) and time dependent square modulus of the harmonic dipole (dashed line). The coherence length decreases rapidly with ionization, giving rise to a propagation term that favors harmonic generation early on the rising edge of the pulse. The amplitude of the induced harmonic dipole tends to favors the peak of the pulse, as does the harmonic radiation phase which varies as $\alpha\nabla I$. The resulting harmonic flux, shown in thick line, is the compromise among these effects. The harmonic flux is then

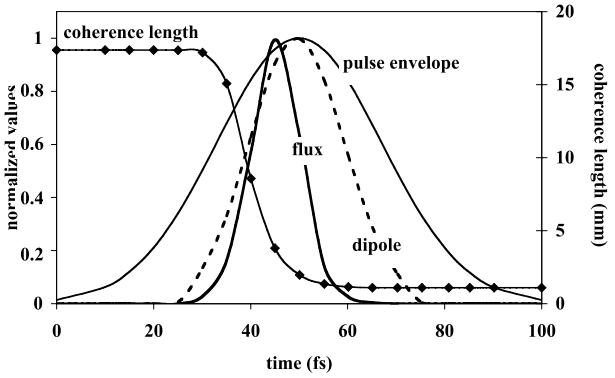

Fig. 7. Simulated time evolution of the parameters influencing the HHG. Thin line: normalized pulse envelope; dashed line: harmonic dipole scaling as I^3 in the plateau region; thick line: harmonic flux, in arbitrary units. The coherence length (full squares) is calculated for the 21st harmonic of argon, 10 mm diameter iris, 10 torr pressure ($L_{\mathrm{abs}} = 1.4$ mm).

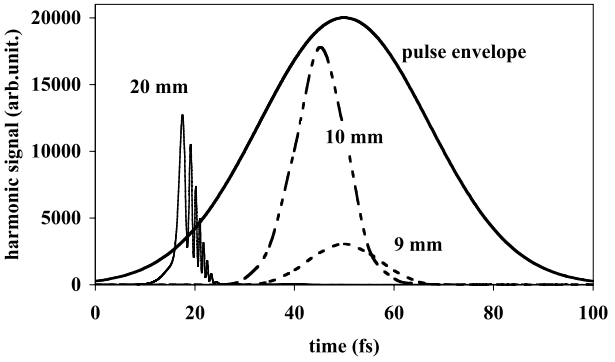

Fig. 8. Time evolution of harmonic flux for different diaphragm apertures compared to the pulse envelope (thick line). Thin line: 20 mm; dashed line: 10 mm; semi dashed line: 9 mm. The experimental conditions are the same as in Figure 4.

integrated over the pulse duration. This one dimensional result is finally weighted by the transverse parameter πw^2 as explained above, to yield the (dimensionless) prediction of the harmonic signal. All the theoretical curves presented were obtained using the values of the intensity and Rayleigh range calculated for each diaphragm value, as discussed in Section 3.2.

4.2 Aperture-dependent intensity effects and temporal profile of harmonic emission

We first investigate how the intensity variations at focus due to aperturing affect the harmonic generation process. A numerical study was thus made of time-dependent one dimensional HHG for three characteristic aperture diameters of the curve in Figure 4: the aperture giving the maximum signal, and for smaller and larger apertures. Figure 8 displays the time evolution of the on-axis harmonic flux (thin continuous, double dashed and simple dashed lines for iris diameters of 20, 10 and 9 mm respectively), with respect to the pulse envelope (thick line). It clearly appears that harmonics are generated earlier in the pulse when the diaphragm is opened but with variable harmonic yields. Coherence length and harmonic dipole considerations allow us to explain this effect.

For large diaphragms, the harmonic flux peaks early on the rising edge of the pulse. This is the result of higher ionization levels, which spoil phase matching, and deplete the neutral medium. The resulting time profile of the harmonic then displays multiple short ripples, with maxima when the cell length happens to correspond to an odd number of the rapidly decreasing coherence length. This complicated time structure, and the rapidly increasing laser intensity at the time of harmonic emission, explain the complex spectra measured experimentally for large diaphragms, as evidenced in Figure 1.

The optimal harmonic emission corresponds to a time profile of harmonic emission much more centered with respect to the pulse envelope, with no secondary maxima of phase matching, and little depletion effects. Two effects contribute to increase the harmonic yield: the increased effective coherence length at the time of the maximum photon flux, mostly related to the larger Gouy dephasing length; and the longer duration of the harmonic emission. These effects are counterbalanced by the lower harmonic dipole amplitude; we find that, in our conditions in argon, the first two factors are dominant, leading to an efficiency improvement by closing the aperture, as long as the intensity is high enough to place that harmonic in the plateau.

4.3 Role of the neutral dispersion of the different noble gases

From simple intensity considerations, one would expect to observe the optimal values of diaphragm apertures decrease when the generating gases changes from neon to argon and finally xenon, as the saturation intensities are much lower for heavy noble gases. The behaviour observed experimentally, and reproduced numerically, is actually at odds with this prediction: the turn on of the curve in xenon is much smoother as in neon or argon, and the optimum is to be found at much larger values (15 mm in Fig. 3), under otherwise identical conditions.

Intensity reached at focus is therefore not the key parameter to understand this specific behaviour. In reference [14], two regimes of phase-matching were proposed. In the first one, phase-matching is obtained early in the pulse, or at low intensities, in conditions such that the atomic dispersion counterbalances the Gouy dispersion. Intensities should be kept low enough that non ionization happens. In the second proposed regime, phase-matching is obtained transiently when the electronic dispersion introduced by the gradual ionization counterbalances the atomic dispersion [16]. As the atomic dispersion is quite low for light noble gases, this happens at a few special values of ionization levels, depending on the gas: at 800 nm, those values are 8% in xenon, and only 1% in neon. The differing behaviours of the diaphragm curves show evidence that the dominant phase matching regime is gradually changing from the first to the second mechanism

when going from a light gas (neon) to a heavy one (xenon). Indeed, the optimum in xenon is obtained at quite high intensities, for which there has to be a high level of ionization. However, its larger atomic dispersion allows good phase matching to be maintained with higher ionization levels, up to the moment when electronic and atomic dispersions compensate, and thus for larger laser apertures with higher atomic response.

4.4 Importance of the laser energy: linearity of phase matching

Varying the iris aperture induces many effects on HHG, both geometrical and energetic ones. We studied the effect of laser energy on the optimal conversion efficiency we could obtain as a function of iris aperture. By this way, we could better distinguish the different roles of aperturing the beam. The conditions for the data shown in Figure 5, were chosen to match those for which we observed the very best conversion efficiency in argon with 6 mJ of laser energy: the laser was focused 8mm before the entrance of a 5 mm long gas cell. Under these conditions, an additional phase matching factor comes into play, namely the atomic phase gradient [9,17], that increases the intensity at which phase matching is achieved [19]. In such conditions, the on axis variation of the phase mismatch along the length of the cell differs rapidly from linear, especially for large apertures. The thin dashed lines in Figure 5 show the results of the model using the linear calculations of phase-matching [14,15]. Obviously, it fails to predict correctly the experimental behaviour, especially for large diaphragm apertures. This shows that our linear treatment of the dephasing between harmonic field and polarization within the gas target is an appropriate approximation only when the Rayleigh range is much larger than the cell length. However, when it approaches a value comparable to the cell length, the phase evolution in the gas increasingly diverges from linear and the calculated effective coherence length is inaccurate. A treatment integrating photon flux over the length of the cell improves the fidelity of the simulation for large apertures, as shown by the line in circles. This improved model reproduces perfectly the general shape of the curves. However, it turned out to fail to predict correctly the relative signal levels; this is due to the simple way in which we took into account the transverse aspect of the harmonic generation: the quantitative influence of the total laser energy on the transverse parameter is there required. In order to scale the theoretical curves, we have hence performed a series of experimental measurements with one fixed diaphragm aperture, but with variable laser energy. The result was used to infer a transverse-surface scaling ratio. This simple 1D model does not take into account 3D phase matching effects that could occur off axis at high energies and generate for example annular harmonics [21]. Nevertheless the results displayed in Figure 5 show excellent agreement with the experimental diaphragm curves. We explain this good agreement by the fact that our harmonic detector is not designed to correctly capture very divergent harmonic emission.

5 Conclusion

The apparent simplicity of aperturing a beam may prevent from considering the full complexity of using a radially truncated beam for HHG, but the effects of an aperture on HHG are multiple, coupled, and non-trivial. We have presented data showing the optimization of HHG signal levels as a function of aperture size, and provided an analysis of the effects of the aperture on HHG. This analysis is based on a simple numerical model which closely matches our experimental curves, and hence allows one to predict the value of the optimum diaphragm aperture for given laser characteristics. In particular, we have shown that the time profile of the emission varies strongly with the iris aperture, as well as the coherence length at the time of maximum flux. In heavy noble gases like xenon, the optimum aperture is relatively large corresponding to high intensities for which there is a balance between electronic and atomic dispersion. In contrast, light noble gases achieve optimum phase matching for lower ionization levels. Finally, we have shown that the phase matching calculations of references [14,15] are only valid when the cell length is small compared to the laser Rayleigh range.

We hope that this analysis will help designing and operating HHG-based short-wavelength light sources for the numerous applications in the growing field of ultrafast XUV optics.

References

1. A. Rundquist *et al.*, Science **280**, 1412 (1998)
2. M. Nisoli *et al.*, Phys. Rev. Lett. **88**, 033902 (2002)
3. D. Descamps *et al.*, Phys. Rev. A **64**, 031404 (2001)
4. Y. Tamaki *et al.*, Phys. Rev. A **62**, 063802 (2000)
5. N.B. Delone, V.P. Krainov, Phys. Usp. **41**, 469 (1998)
6. R.D. Cowan, *The theory of atomic structure and spectra* (The university of California, 1981)
7. M. Lewenstein *et al.*, Phys. Rev. A **49**, 2117 (1994)
8. M. Lewenstein *et al.*, Phys. Rev. A **52**, 4747 (1995)
9. Ph. Balcou *et al.*, Phys. Rev. A **55**, 3204 (1997)
10. A. Siegman, *Lasers* (The university of California, 1986), p. 666
11. D.G. Lee *et al.*, Phys. Rev. Lett. **87**, 243902 (2001)
12. A. Siegman, *Lasers* (The university of California, 1986), p. 727
13. R.K. Tyson, *Adaptative optics engineering handbook* (Marcel Dekker, Inc., 2000) 123
14. C. Durfee *et al.*, Phys. Rev. Lett. **83**, 2187 (1999)
15. E. Constant *et al.*, Phys. Rev. Lett. **82**, 1668 (1999)
16. M. Schnürer *et al.*, Phys. Rev. Lett. **83**, 722 (1999)
17. P. Salières *et al.*, Phys. Rev. Lett. **74**, 3776 (1995)
18. Technical details can be found on: `http://www.oxalis-laser.com`
19. S. Kazamias *et al.*, to be published
20. Ph. Balcou *et al.*, J. Phys. B: At. Mol. Opt. Phys. **32**, 2973 (1999)
21. P. Salières *et al.*, Adv. At., Mol. Opt. Phys. **41** (1999)